Published in final edited form as:
Biochemistry. 2009 August 25; 48(33): 7996–8005. doi:10.1021/bi901037u.

Effect of Active-site Mutation at Asn67 on the Proton Transfer Mechanism of Human Carbonic Anhydrase II

C. Mark Maupin[§,≠], **Jiayin Zheng**[‡,≠], **Chingkuang Tu**[‡], **Robert McKenna**[†,*], **David N. Silverman**[†,‡,*], and **Gregory A. Voth**[§,*]

[§]Center for Biophysical Modeling and Simulation and the Department of Chemistry, University of Utah, Salt Lake City, UT 84112

[‡]Department of Pharmacology and Therapeutics, University of Florida, Gainesville, FL 32610

[†]Department of Biochemistry and Molecular Biology, University of Florida, Gainesville, FL 32610

Abstract

The rate-limiting proton transfer (PT) event in the site-specific mutant N67L of human carbonic anhydrase II (HCA II) has been examined by kinetic, x-ray, and simulation approaches. The x-ray crystallography, which were previously reported, and molecular dynamics (MD) simulations indicate that the proton shuttling residue, His64, predominantly resides in the outward orientation with a significant disruption of the ordered water in the active site for the dehydration pathway. While disorder is seen in the active-site water, water cluster analysis indicates that the N67L mutant may form water clusters similar to those seen in the wild-type (WT). For the hydration pathway of the enzyme, the active site water cluster analysis reveals an inability of the N67L mutant to stabilize water clusters when His64 is in the inward orientation, thereby favoring PT when His64 is in the outward orientation. The preference of the N67L mutant to carry out the PT when His64 is in the outward orientation for both the hydration and dehydration pathway is reasoned to be the main cause of the observed reduction in the overall rate. To probe the mechanism of PT, solvent H/D kinetic isotope effects (KIEs) were experimentally studied with catalysis measured by the exchange of ^{18}O between CO_2 and water. The values obtained from the KIEs were determined as a function of the deuterium content of solvent, using the proton inventory method. No differences were detected in the overarching mechanism of PT between WT and N67L HCA II, despite changes in the active-site water structure and/or the orientation of His64.

Keywords

Carbonic anhydrase; Carbon dioxide; Proton transfer; Oxygen-18; Isotope exchange; mass spectrometry; Molecular dynamics; Path integral molecular dynamics

Human carbonic anhydrase II (HCA II) is a zinc-metalloenzyme that catalyzes the reversible hydration and dehydration of carbon dioxide and bicarbonate (Eqs. 1 and 2):[1-3]

*Corresponding authors: G.A.V. Center for Biophysical Modeling, Department of Chemistry, University of Utah, Salt Lake City, UT 84112, Phone: (801) 581 5419; Fax (801) 581 4353; voth@hec.utah.edu; D.N.S. Department of Pharmacology, College of Medicine, University of Florida, Box 100267, Gainesville, Florida 32610; Phone: (352) 392 3556; Fax (352) 392 9696; silvrmn@ufl.edu; R.M. Department of Biochemistry and Molecular Biology, College of Medicine, University of Florida, Box 100245, Gainesville, Florida 32610; Phone: (352) 392 5696; Fax: (352) 392 3422; rmckenna@ufl.edu.
[≠]CMM and JZ contributed equally to this work.

Supporting Information Available: Supplemental Figure 1 depicting the $\chi 1$ and $\chi 2$ sampling for His64 in the NMPIMD simulations. Discussion of how the character of the hydronium cation, Eigen or Zundel, may impact the KIE. This material is available free of charge via the Internet at http://pubs.acs.org.

$$CO_2 + EZnOH^- \rightleftarrows EZnHCO_3^- \overset{+H_2O}{\underset{-H_2O}{\rightleftarrows}} EZnH_2O + HCO_3^- \quad (1)$$

$$His64 - EZnH_2O + B \rightleftarrows H^+His64 - EZnOH^- + B \rightleftarrows His64 - EZnOH^- + BH^+ \quad (2)$$

Here, B is an exogenous proton acceptor from solution. The rate-limiting step in the maximal velocity of catalysis by HCA II under well-buffered conditions is the active-site water proton transfer (PT) of Eq. 2, in which the solvent-accessible residue His64, positioned along the side of the active-site cavity, acts as the proton shuttle in the catalysis.[4-6]

The side chain of His64 is about 8 Å away from the zinc.[7, 8] This distance is too great for direct PT between His64 and the zinc-bound solvent molecule. Therefore, the proton transfer is hypothesized to be dependent on the water structure in the active-site cavity in a concerted or step-wise mechanism.[9, 10] X-ray crystallography of wild-type (WT) HCA II shows 60%-80% inward (His64 directed toward the active site) versus outward (His64 directed away from the active site) for pHs ranging from 6 to 8.[8, 11]

In WT HCA II there are several amino acids extending into the active-site cavity with side chains 6 – 8 Å from the zinc. These residues (Tyr7, Asn62, and Asn67) are believed to be critical to the stabilization of the active-site water network consisting of Zn-H_2O/OH^-, W1, W2, W3a, and W3b (Figure 1A).[11-13] Measures of the rate of catalysis, combined with analysis of the x-ray crystal structures of mutants at these positions, have shown changes in the side-chain orientation of His64, in the pK_a of the imidazole of His64, and in ordered water structures of the active-site cavity.[12] In N67L HCA II crystals, the His64 side chain is completely in the outward orientation and the active-site water network is disrupted (Figure 1B). In this enzyme, the pK_a for His64 (pK_a 7.5) was elevated by about one pK unit above that of the wild type, and the rate constant for PT was four times less than that for WT HCA II.[12]

In light of the aforementioned observations, this study seeks to understand the effects of changes in the structure of ordered water and the orientation of His64, as observed in the crystal structures, on catalysis through the lens of molecular dynamics (MD) simulations. Specifically, the goal of this work is to help understand how the mutant enzyme N67L HCA II, with no organized active-site water in the crystal structure and the His64 side chain oriented away from the active site, can still generate a significant rate of catalytic PT, only four times less than that of WT HCA II. In order to do this, proton inventory, the dependence of the kinetics of catalysis on the atom fraction of deuterium in solvent, was investigated.[14] Such a proton inventory study is sensitive to the number of protons transferred in catalysis by carbonic anhydrase.[15] In addition to the kinetic studies, MD simulations are used to determine the potential of mean force (PMF) for the rotation of His64 about the χ1 dihedral (N-Cα-Cβ-Cγ). These simulations, in conjunction with x-ray crystallographic data, give insight into the orientational distribution of His64. MD simulations are also used to evaluate the stability of the active-site water cluster for both forms of the enzyme (i.e. hydration and dehydration pathway), with His64 in either the inward or outward orientation. Such atomistic structural data allows for a detailed analysis of the active-site water cluster, which is considered to be an integral part of the rate-limiting PT step.[6, 13] To evaluate the effects of deuterium on the active-site water cluster, quantum path integral molecular dynamics (PIMD) simulations were conducted in which the nuclear motion is quantized. These simulations reveal the differences in the formation and stabilization of the active-site water cluster during KIE experiments.

Materials and Methods

Expression and Purification of Enzymes

The mutant N67L of HCA II was made by site-directed mutagenesis using expression vectors containing the HCA II coding region.[4, 16] A plasmid with the mutation N67L in cDNA of HCA II was made by site-directed mutagenesis using the QuikChange II Kit (Stratagene, La Jolla, CA). The sequence of this mutant was confirmed by sequencing the DNA of the entire coding region for carbonic anhydrase (CA) in the expression vector. Expression of the mutated vector was done by transforming into *Escherichia coli* BL21 (DE3) pLysS, which does not express any indigenous CA under these conditions. Purification was performed by affinity chromatography using *p*-(aminomethyl)benzenesulfonamide coupled to agarose beads.[17] Electrophoresis on a 10% polyacrylamide gel stained with Coomassie Blue was used to confirm the purity, which was greater than 96% for all enzyme samples. The enzyme concentrations were determined by titration of the active sites with ethoxzolamide, which binds tightly to WT and N67L HCA II. Rates of catalysis were measured by the ^{18}O exchange between CO_2 and water, as discussed below, analyzing data with the Henderson approach.[18]

Oxygen-18 Exchange

This method of rate determination is based on the depletion of ^{18}O from species of CO_2 as measured by membrane inlet mass spectrometry.[19, 20] CO_2 passing across the membrane enters a mass spectrometer (Extrel EXM-200), providing a continuous measure of isotopic content of CO_2. In the first stage of catalysis, the dehydration of labeled bicarbonate has a probability of transiently labeling the active site with ^{18}O (Eq.3). In a subsequent step, the protonation of the zinc-bound ^{18}O-labeled hydroxide results in the release of $H_2{}^{18}O$ to the solvent (Eq. 4)

$$HCOO^{18}O^- + EZnH_2O \underset{+H_2O}{\overset{-H_2O}{\rightleftarrows}} EZnHCOO^{18}O^- \rightleftarrows COO + EZn^{18}OH^- \tag{3}$$

$$H^+His64 - EZn^{18}OH^- \rightleftarrows His64 - EZnH_2{}^{18}O \underset{-H_2O}{\overset{+H_2O}{\rightleftarrows}} His64 - EZnH_2O + H_2{}^{18}O \tag{4}$$

This approach yields two rates for the ^{18}O exchange catalyzed by carbonic anhydrase.[19] The first is R_1, the rate of exchange of CO_2 and HCO_3^- at chemical equilibrium, as shown in Eq. 5. Here k_{cat}^{ex} is a rate constant for maximal interconversion of substrate and product; K_{eff}^{S} is an apparent binding constant for substrate to enzyme; and [S] is the concentration of substrate, either CO_2 or bicarbonate.[21] The ratio k_{cat}^{ex}/K_{eff}^{S} is, in theory and in practice, equal to k_{cat}/K_m obtained by steady-state methods.

$$R_1/[E] = k_{cat}^{ex}[S]/(K_{eff}^{S} + [S]) \tag{5}$$

A second rate determined by the ^{18}O-exchange method is R_{H_2O}, the rate of release from the enzyme of water-bearing substrate oxygen (Eq. 4). This component of the ^{18}O exchange is dependent upon the donation of protons to the ^{18}O-labeled zinc-bound hydroxide.[4, 19] In this step, His64 is the predominant proton donor in the catalysis (Eq. 4). The value of R_{H_2O} can be interpreted in terms of the rate constant for PT to the zinc-bound hydroxide according to Eqs. 4 and 6, in which k_B is the rate constant for PT to the zinc-bound hydroxide, and $(K_a)_{donor}$ and

$(K_a)_{ZnH2O}$ are the ionization constants of the proton donor and zinc-bound water molecule. The kinetic constant k_B and ionization constants of Eq. 6 were determined by nonlinear least-squares methods (Enzifitter, Elsevier-Biosoft, Cambridge, U.K.)

$$k_B^{obs} = k_B / \left(\left[1 + (K_a)_{donor} / [H^+] \right] \left[1 + [H^+] / (K_a)_{ZnH_2O} \right] \right) \quad (6)$$

Unless stated otherwise, the uncatalyzed exchange and the carbonic-anhydrase-catalyzed exchange of ^{18}O between CO_2 and water at chemical equilibrium were measured in the presence of buffer at a total substrate concentration of 25 mM, using membrane-inlet mass spectrometry.[19] The temperature was 25 °C and the total ionic strength of the solution was kept at a minimum of 0.2 M by the addition of Na_2SO_4. Deuterium oxide (99.9% D_2O) was obtained from Sigma-Aldrich and distilled from activated charcoal before use.

Molecular Dynamics Simulations

All simulation systems were based on the WT HCA II x-ray structure with a resolution of 1.54 Å (PDB accession # 2CBA).[22] The N67L mutant was created by using the Swiss-PDB Viewer[23] to mutate Asn to the most appropriate rotamer of Leu. This mutation was simulated for both the hydration and dehydration of HCO_3^-. The hydration system contained a zinc-bound water and an unprotonated His64 (ZnH_2O^{2+}-His) and was modeled with His64 in both inward and outward orientations. The dehydration system contained a zinc-bound hydroxide and a protonated His64 ($ZnOH^+$-$HisH^+$), and was modeled with His64 in the outward position only. The choice to model only the outward orientation for the dehydration system was based on the results from the N67L χ1 dihedral PMF for His64 (described below) and on recent x-ray results (PDB accession # 2NWY and 2NWZ).[12] The 2CBA x-ray crystal was used as the template for the MD simulations rather than the 2NWY or 2NWZ crystal structures, as both x-ray and MD simulation research projects were being conducted independently at the same time.[12] The N67L mutant of HCA II along with the 220 x-ray waters were then solvated in a cubic box (L ≈ 75 Å) of modified TIP3P water.[24] The parm99[25] force field was used to describe the enzyme, while the active site was described by the parameters used in Maupin and Voth.[26] The ZnH_2O^{2+}-His and the $ZnOH^+$-$HisH^+$ systems were equilibrated for 250 ps in the constant NVE ensemble, followed by a 1.0 ns equilibration run in the constant NPT ensemble.[27] Data were then collected from a 2.0 ns simulation in the constant NVT ensemble.[27] All simulations used periodic boundary conditions. Long-range Coulomb interactions were calculated by a particle-mesh Ewald summation, while short-ranged, non-bonded interactions and forces were subject to a 10 Å cutoff.[28] The enzyme simulations were conducted at 298.15 K and used the leap-frog Verlet integrator with a time step of 0.5 fs. The NPT ensemble simulations were conducted at 1 atm; all constant-temperature simulations used Langevin dynamics for the thermostat.

Normal Mode Path Integral Molecular Dynamic (PIMD) Simulations

PIMD simulations were conducted to evaluate the quantum effects of deuterium on the structure of the active-site water cluster. PIMD is a computationally efficient method for calculating the equilibrium properties of a quantum many-body system. The use of PIMD methods to calculate PT isotope effects in aqueous[29] and enzyme systems,[30, 31] including the WT HCA II,[32] have been carried out by others. However, the use of PIMD in the current study is restricted to an exploration of the structural characteristics of the active site water cluster. An explicitly reactive potential is not used in this work in an effort to calculate actual PT rates. The present simulations were carried out using the normal mode path integral molecular dynamics (NMPIMD) methodology implemented in AMBER 10.[33] The fundamentals of PIMD have been covered in detail elsewhere and therefore will not be described here.[34, 35] The initial coordinates for the NMPIMD simulations were taken from the final step of the MD

data collection simulations. The NMPIMD simulations were then quantized using 16 path integral quasi particles per physical particle. The systems were equilibrated for 25 ps in the constant NVT ensemble, followed by 1 ns of data collection. A Nosé-Hoover chain thermostat coupled to each degree of freedom was used to keep the system temperature at 298.15 K.[36] The leapfrog integrator was used to propagate the system with a time step of 0.5 fs. The water model used in the simulations was a simple point charge, flexible water model specifically developed for investigations of nuclear quantum effects.[37] To approximate deuterium, the mass of all labile hydrogens, on water and amino acids, was set to 2.014 g/mole in all simulations.

Active Site Water Cluster Analysis

The previously outlined unbiased MD simulations were analyzed for continuous water clusters connecting the zinc-bound water to His64 in the hydration systems or the zinc-bound hydroxide to $His64H^+$ in the dehydration systems. The active-site water cluster is defined as a continuously hydrogen-bonded network of water in which (a) the donating and accepting oxygens are within 3.5 Å of each other; (b) the acceptor oxygen and the donating oxygen's hydrogen are within 2.5 Å; and (c) an angle of less than 120° exists between the donating oxygen-donating hydrogen vector and the donating oxygen-accepting oxygen vector. The water cluster distribution was further analyzed by determining the smallest water cluster, given that a water cluster is present. In addition to the distribution of water cluster sizes, the water cluster lifetimes were evaluated for each participating water cluster size. In all calculations, the zinc-bound water and zinc-bound hydroxide are included in the water cluster size and lifetime count. For the evaluation of the NMPIMD simulations, the water cluster analysis was conducted on each of the quasiparticles and then averaged over the quasiparticles to obtain the final result. Since NMPIMD does not yield dynamical information, the water cluster lifetime was not evaluated for those simulations.

Active Site Water Occupancy Analysis

Active-site water occupancy analysis was conducted on the previously outlined unbiased MD simulations to determine the stability of the active-site waters for the hydration and dehydration systems. To evaluate the stability of the active-site waters, each system was first centered and fitted with a nonlinear least squares method to the average configuration. After orienting the simulations to a common reference, the Volmap tool in VMD[38] was used to generate the average occupancy of the water oxygens in the active site. The average occupancy of the active-site water clusters was analyzed at both the 50% and 75% occupancy isosurfaces.

Umbrella Sampling Simulations

The umbrella sampling biased simulation procedure was used to evaluate the potential of mean force (PMF) profile for rotating the His64 about the χ1 dihedral angle.[26] This procedure was chosen because the barrier of rotation between the inward and outward orientation was larger than k_BT. To more thoroughly sample areas corresponding to relatively large free energy, an umbrella potential of the form

$$U_n^{\text{umbrella}}(\xi_{\chi 1}) = \frac{k_n}{2}(\xi_{\chi 1} - \xi_0^n)^2 \tag{7}$$

was used to restrain the sampling of the dihedral angle. A dihedral force constant, k_n, of 40 kcal mol^{-1} rad^{-2} was placed on ten windows spaced equidistantly over a range of $\xi_0^n = -100°$ to 100°. The initial umbrella sampling simulation conformations were taken from the final classical MD configuration of the unbiased simulations. The windows were then equilibrated for 500 ps followed by a data collection period of 1 to 2 ns in the constant NVT ensemble,

depending on convergence. The MD time integration step and the temperature were set to 1 fs and 298.15 K, respectively. The biased sampling data were then recombined using the weighted histogram analysis method[39, 40] (WHAM) to generate a continuous PMF curve for the rotation of His64 about the χ1 dihedral angle.

Results

Solvent Hydrogen Isotope Effects (dehydration)

The pH profile of the rate constant R_{H_2O}/[E] catalyzed by N67L HCA II in H_2O, which has been reported previously (Figure 3 of Fisher et al.[12]), was bell-shaped, similar to the pH profile for WT HCA II.[41] This experiment was repeated for different atom fractions of deuterium in solvent. The resulting pH profiles were fitted using Eq. 6 to provide estimates of the pK_a for the donor (His64) and acceptor (zinc-bound water), and the rate constant k_B for PT. These values in H_2O were $(pK_a)_{His64}$ = 7.7 and $(pK_a)_{ZnH_2O}$ = 6.4; the changes in these values in 99.8% D_2O were $\Delta(pK_a)_{His64}$ = 0.7 and $\Delta(pK_a)_{ZnH_2O}$ = 0.3 ($\Delta pK_a = (pK_a)_{D_2O} - (pK_a)_{H_2O}$). These values fall within the range of solvent H/D isotope effects on the ionization constants of well-behaved acids (Table II of [ref. 13]).

The proton inventory plot for k_B for catalysis by the mutant N67L HCA II is shown in Figure 2. The overall H/D kinetic isotope effect (KIE) on k_B ($k_{B,H_2O}/k_{B,D_2O}$) observed for N67L HCA II was 4.6 ± 0.5, large enough for an interpretable proton inventory plot. The comparable KIE for WT HCA II, obtained from previously reported proton inventory experiments, is 3.8 ± 0.6.[5, 15] The overall H/D KIEs on R_1/[E] for N67L and WT HCA II were 1.2 ± 0.1 and 1.2 ± 0.1, respectively. These results indicate no rate-contributing PT in the first stage of catalysis (Eq. 1) for either the WT or N67L mutant. That is, these isotope effects are consistent with direct nucleophilic attack of the zinc-bound hydroxide on CO_2 for both WT and N67L HCA II.

Orientational Stabilization of His64 in the N67L mutant (hydration and dehydration)

The PMFs for the rotation of His64 about the χ1 dihedral angle for the hydration and dehydration systems of N67L HCA II are shown in Figure 3 (A and B, respectively). The N67L mutant for the hydration system has increased the orientational mobility of His64 around the χ1 dihedral, yielding an approximate 50/50 inward/outward distribution. It is apparent that this mutation has significantly affected the orientational stability of His64 relative to the WT system, in which the distribution is 80% inward.[26] In addition to the χ1 dihedral, the χ2 dihedral also shows an increased sampling while in the inward orientation compared to WT. These changes to the χ1 and χ2 dihedral sampling in the N67L mutant indicate a reduced ability of the active-site water to stabilize His64 in the inward orientation as compared to WT.

For the dehydration pathway, both the WT[26] and the N67L mutant (Figure 3B) prefer the outward orientation significantly more than the inward. In addition to the χ1 dihedral, the χ2 dihedral possesses very similar sampling patterns to the WT. These results reveal that the N67L mutant does not significantly affect the dehydration system, which indicates that the PT for this system may be similar to that of WT.

The x-ray crystal structures for the N67L mutant (PDB accession # 2NWY and 2NWZ)[12] show the His64 almost exclusively in the outward orientation, which agrees very well with MD simulations of the dehydration system. Given that the N67L HCA II x-ray crystal structures were studied at pHs of 8.2 and 6.0 (2NWY and 2NWZ, respectively), and that kinetic experiments determined the pK_a of the ZnH_2O to be near 6.0,[12] the probability that the crystal structures are represented by the dehydration system ($ZnOH^-$) is significant (especially for

2NWY). Taken together, the kinetic and x-ray crystallographic data show excellent structural agreement between experiment and simulation.

In addition to the protium simulations, deuterium simulations (unbiased NMPIMD) of the N67L HCA II hydration (inward and outward) and dehydration (outward) systems were conducted. Evaluation of the χ1 dihedral sampling for the deuterium systems for both the hydration and the dehydration systems indicated no significant effect of deuterium substitution on the sampling of the χ1 dihedral angle (data not shown). As with the χ1 dihedral sampling, deuterium in the outward orientation of the dehydration system had no significant effect on the χ2 dihedral sampling. Unlike the dehydration system, the χ2 dihedral sampling for the deuterium hydration system indicates minor perturbations when compared to the protium system (Supplemental Information). These perturbations are due to differences in the strength of the deuterium and protium hydrogen bonds.[42, 43]

Active Site Water Cluster Formation and Lifetime Analysis

The distribution of water cluster sizes in the active site of the N67L HCA II mutant is shown in Figure 4A. The peak of this distribution shows the size of water clusters that a particular enzyme prefers to form, and gives insight into which water cluster is most important in the rate-limiting PT event. For the N67L mutant in the hydration system with His64 in the inward orientation, the water clusters range from 3 to 10 molecules. The presence of clusters containing 3 or 4 water molecules is similar to the results for the WT HCA II enzyme.[13, 44] Both the hydration and dehydration systems in the outward orientation of the N67L mutant contain water clusters of 5 to 10 molecules, due to His64 residing at a greater distance from the zinc-bound water/hydroxide. Both outward-oriented systems have their most probable water clusters at larger sizes, 8 and 6 for the hydration and the dehydration system respectively. The relatively large standard deviations of these distributions indicate significant instability in the active-site water cluster, a characteristic not shared by the catalytically more efficient WT HCA II.[13]

To study the effect of deuterated solvent, the cluster sizes of D_2O molecules in the active site of N67L HCA II were examined (Figure 4B). It is evident that in the deuterium system the variability seen in the protium clusters is largely eliminated. The reduction in variability is due to the stronger deuterium bonds (d-bonds) in D_2O as compared to H_2O (h-bonds). The overall distribution of sizes in the D_2O clusters is similar to that of the H_2O clusters discussed earlier. Analysis of the deuterium clusters for the inward orientation of the N67L HCA II hydration system reveals that the smaller cluster sizes are very rare, which indicates that this mutation has significantly affected the ability of the enzyme to form and stabilize smaller cluster sizes (sizes 3 and 4).

Lifetimes can also yield important information on the stability and probable efficiency of these water clusters in facilitating the PT event. The data on water cluster lifetimes for the N67L mutant are found in Figure 5. The lifetimes of water clusters for the hydration system are markedly different than those of the WT. For the N67L mutant, the lifetimes of water clusters do not exceed 1 ps; while for WT, they can last as long as 3 to 6 ps. This indicates that the N67L mutation has altered the ability of the water clusters to form in the active-site cavity. The outward orientations for both the hydration and dehydration systems in N67L possess lifetimes that are similar to those of the WT HCA II. Along with the cluster size results, this result indicates that the N67L mutation affects the inward orientation of the hydration system predominantly by significantly reducing the formation and lifetime of the active-site water clusters, whereas the outward orientations of both the hydration and dehydration systems are relatively unaffected. (The lifetime calculations were not performed on the NMPIMD simulations due to the fact that dynamical data cannot be obtained from such simulations.)

Active Site Water Cluster Occupancy

The water cluster occupancy data depict the positions and relative stability of the active-site H_2O and D_2O clusters. The occupancy data for the classical MD simulations can be found in Figure 6. For the quantum NMPIMD simulations, negligible differences were found between deuterium and protium system occupancies. The water occupancy levels for the inward orientation of the hydration system of N67L HCA II and the equivalent WT system are strikingly similar. It appears from Figure 6A that the N67L mutation has not disrupted the occupancy of the active-site water cluster. This result is in contrast with the water cluster formation and lifetime data, both of which indicate a disrupted water cluster. Upon closer inspection of the atomistic details, it is found that the spatial orientation of the waters in the water cluster is disordered for the N67L mutant. The N67L mutation has affected the hydrogen bonding orientation found in the water cluster, specifically between W1, W2, W3b, and W3a (Figure 6A). The atomistic analysis revealed that these waters rarely hydrogen bond to one another. In the instances when hydrogen bonding does occur, the water clusters typically are not directional, that is, they may not be as capable of transferring an excess proton in a singular direction.

Correlation Analysis for the Active Site Water Cluster and Stabilizing Amino Acids

Correlation analysis of the active-site water cluster and critical amino acids in the active site of the N67L mutant allows for a better understanding of the complex interplay of hydrogen bonding and enzyme fluctuations. These long and short range correlations between species may stabilize or destabilize the active-site water cluster. A correlation analysis for the entire hydration system, including both inward and outward orientations of His64, is found in Figure 7. The most evident feature of Figure 7A is an absence of significant correlations in the active site as compared to the WT.[13] There appears to be a small correlation between W2, W_D, and the ZnH_2O. It is evident that the N67L mutation has disrupted the ability of the active-site amino acids to affect the water cluster to a significant degree. Another difference between the WT and the N67L HCA II is the lack of correlation between the active-site water cluster and W_D in the N67L mutant. Due to the fact that hydrogen-bonded species generally have high degrees of correlation, the correlation patterns for the N67L mutant indicate that the hydrogen-bonding network has been disrupted in the active site.

When looking at the outward orientation of the dehydration system of the N67L mutant, a significantly different pattern of correlation can be seen when compared to the previous correlation analysis. Figure 7B clearly reveals significant levels of positive correlation between amino acids and the active-site water cluster, and between waters inside the active-site water cluster. A point of interest is water W1*, which does not correspond to water W1 in the WT. W1* resides near the top of the active site, above the position typically occupied by W1. While this water can donate a proton to the Zn-bound hydroxide, it does not reside in the typical water cluster chain, which is stabilized by Thr199 and Thr200. The correlation level in the outward orientation of the dehydration system reveals that the hydrogen-bonding network has been somewhat restored, indicative of a system that is capable of PT.

Discussion

The aim of this work is to pursue a more complete understanding of the kinetics of PT in HCA II, specifically in relation to two structural features in the active-site cavity of WT HCA II: the ordered water cluster and the orientation of the side chain of His64. The N67L HCA II mutant was chosen for two characteristics: its lack of ordered water in the active-site cavity, and the outward orientation of its His64 side chains, as seen in the x-ray crystal structure.[12] The fundamental question of interest is how the N67L mutant, with these substantial structural differences from WT, could maintain a rate of PT in catalysis, 0.2 μs^{-1} (Figure 2), that is only

four times less than that of WT HCA II and posses a similar mechanism for PT (similar KIE and proton inventory to WT). Kinetic experiments (KIE and proton inventory), x-ray crystal structures, and MD simulations of the $ZnOH^+$-$HisH^+$ system are used to evaluate the dehydration pathway, whereas the hydration pathway is evaluated solely through simulations of the ZnH_2O^{2+}-His system. Through these detailed analyses, a more complete understanding of the kinetics and atomistic structural properties of the N67L mutant is achieved. Our data elucidate the role and significance of the ordered water structure and the orientation of His64 in catalysis by carbonic anhydrase.

Dehydration pathway ($ZnOH^+$-$HisH^+$)

Orientation of His64—While the proton acceptor/donor His64 is believed to play a fundamental role in the PT event,[16] an understanding of how its orientation (inward vs. outward) affects the rate-limiting PT event has, so far, been elusive. Recent kinetic and x-ray studies have shown that allowing orientational freedom (i.e., the ability to adopt both inward and outward orientations) results in an enzyme with a PT rate similar to that of WT HCA II, while restricting the orientational freedom of His64 (i.e., only inward or outward orientations are permitted) has a detrimental effect on the observed rate.[45] In these studies, restricting His64 to the outward orientation reduces the rate to a larger degree than restricting His64 to the inward orientation. While these results seem to indicate a straightforward relationship between His64 orientation and the observed rate, there are other mutations which defy such simple explanations.[12, 46] Recent computational work has even predicted that the orientation of His64 does *not* influence the observed rate.[47] Conflicting results such as these have hampered the efforts of experimentalists and theorists alike in determining the exact role of the orientation of His64 on the observed rate. Clearly, it seems evident that a more thorough evaluation of the orientation of His64 and its impact on the active-site water cluster and PT is needed.

Understanding the orientational preference of His64 is a crucial first step to clarifying the role of its orientation on the observed rate. To this end, x-ray and simulation data were used in the present work to gain insight into the orientation preference of His64 in the N67L mutant. X-ray data on the N67L mutant indicate that the side chain of His64 occupies the outward orientation almost exclusively.[12] Given the pH of the crystal and the pK_a of the zinc-bound water and His64, it is reasoned that the x-ray data is indicative of the dehydration system. In an effort to expand on the x-ray data, MD simulations for the dehydration system of the N67L mutant were conducted. The orientational stability of His64 in the N67L mutant, as determined by the PMF for the $\chi 1$ dihedral angle (Figure 3B), reveals that the side chain of His64 is almost always in the outward orientation. This result agrees with the crystal structure x-ray data. Thus, the outward orientation of His64 is predominant in the dehydration system, a results also seen in the MD simulation work on the WT and Y7F mutant HCA II.[13, 26]

To gain a better understanding of the factors that are influencing the observed rates, the characteristics of the active-site water cluster, believed to be important in the rate-limiting PT event, were also evaluated. While the x-ray data yield the positions of water oxygens, they do not provide information on the water cluster size distribution, orientations, and/or lifetimes, all of which are important to understanding the effect of His64's orientation on the active-site water. This information could, however, be obtained from the MD simulation data. Taking into account the outward preference of His64 in the N67L mutant, the water cluster size distribution was evaluated and it was found that active-site waters clusters are similar to those found in the WT system, typically 6 water molecules or more (Figure 4B). Cluster lifetimes also indicate negligible differences between WT and the N67L mutant. These results at first seem to contradict the x-ray data, which indicate disorder in the active-site water cluster. To clarify this discrepancy, occupancy data were analyzed (Figure 6) and a correlation analysis (Figure 7B) was conducted. The occupancy data revealed a level of disorder in the oxygen positions quite

similar to that seen in the x-ray data. Thus, although there is disorder in the water positions, it appears that continuously hydrogen-bonded water clusters may still form and exist for an appreciable amount of time. To explore this possibility, the correlation analysis was used to inspect possible stabilizing interactions. It was found that similar levels of stabilizing hydrogen bonding were occurring in the N67L mutant and the WT systems. Together, these data point to the creation of hydrogen bonding networks in both systems, albeit through different types of water clusters, which on average are stabilized by the active site environment.

The above results shed light on the possible ways in which the HCA II enzyme can adjust to various mutations. It also suggests that the presence of static disorder in the water positions does not necessarily preclude the formation of dynamic water clusters. Indeed, as seen in the WT and N67L mutant, water clusters can still form by various pathways. In addition to helping explain how the N67L mutant retains a rate similar to WT, these results stress the reduced importance of specific water clusters in the transfer of the proton from donor to acceptor when His64 is in the outward orientation. While the presence of water clusters is still important, their role is changed in the N67L system. Water clusters are dynamic, and PT is not necessarily restricted to a specific type of cluster. This degree of freedom appears to be related to the distance between donor and acceptor, in that longer paths increase the importance of the diffusive nature of the excess proton. It should be stressed that the water cluster size and lifetimes likely play a larger role when His64 is in the inward as compared to the outward orientation. With this view of the intricate interplay between the orientation of His64 and the water cluster characteristics, it seems clear that the N67L mutant, while modifying the orientation of His64, does not have a significant impact on the water cluster distribution. It should be noted that the inward orientation for the dehydration pathway was not studied due to its very low probability of occurrence of ≤ 10% in the x-ray data, and ≤ 1% in the MD simulations.

Having studied the effect of the N67L mutation on the orientation of His64 and the active-site water clusters, the next step was to determine how these changes might affect the observed PT rate. Considering the similarities in the orientation of His64 and the characteristics of the water cluster between WT and N67L HCA II, the fundamental cause of the four-fold decrease in the observed rate for the N67L mutant can now be addressed. Due to the similarities between the water cluster's characteristics in the WT and N67L mutant, the nature of the PT event in the WT system is likely sufficient to describe the corresponding PT event in the N67L mutant. Recent multi-state empirical valence bond (MS-EVB) simulations of WT HCA II indicate a rate of ~ 0.1 μs^{-1} when His64 is in the outward orientation.[6] Indeed, a four-fold decrease in the rate of PT as seen in kinetic studies of the N67L mutant, which is predominantly in the 'out' configuration, yields a rate of 0.2 μs^{-1}, in good agreement with the aforementioned WT His64 'out' simulation. These results indicate that the fundamental physics that alter the PT free energy barrier in the WT, between His64 in the inward and outward orientation, are also at play in the N67L mutant. It is the greater distance between proton donor and acceptor, necessitating the presence of a larger water cluster, which ultimately influences the observed rate and cause it to be lower in N67L.

Deuterium studies—One of the few experimental ways to assess a possible role for water molecules in the transition state of the PT is through a proton inventory experiment, which evaluates the dependence of the PT rate constant on the atom fraction of deuterium in solvent (denoted *n*).[14] This property of the KIE is sensitive to the participation of water molecules, including the number of protons transferring in the transition state. The proton inventory plot for k_B for the N67L mutant was examined and compared with that of WT HCA II (Figure 2). The overall H/D KIE ratio was near 4 for both for N67L and WT HCA II, consistent with a PT process that is rate-contributing to the same extent for both enzymes. In addition, both proton inventory plots are concave downward and curved to a nearly identical degree. For both

N67L (Figure 2) and WT HCA II (data reported earlier in [ref. 14]), the dependence of k_B on n is very close to logarithmic, consistent with a change in bonding to many hydrogen atoms.[14] Within the precision characteristic of this analysis, a change in fractionation factors by one or two protons in the transition state for N67L can be excluded, consistent with the case for WT HCA II in an earlier report.[15] It is assumed in such studies that the proton motion occurs in the transfer of protons through transiently formed intervening water structures from His64 to the zinc-bound solvent or in the change in bonding to these protons and many other protons of the solvent structure, which may alter H/D fractionation factors of many solvent molecules in the transition state. As the proton inventory results appear the same in the kinetics of PT by WT and N67L HCA II, it is concluded that differences in water cluster characteristics have no significant impact on the proton inventory of these two systems. That is, there is no evidence that N67L and WT HCA II employ different mechanisms of PT (for example, concerted versus step-wise). We again note that the proton inventory method would not be sensitive to changes in bonding to three or more hydrogens.

To explore the kinetic deuterium studies at an atomistic level, NMPIMD deuterium simulations were conducted on the dehydration system and, for completeness, on the hydration system as well. When deuterium studies are used, the similarities of active-site water cluster characteristics for an enzyme in D_2O compared to an enzyme in H_2O must be considered. The data show that deuterated systems and protonated systems result in similar water cluster distributions (Figure 4B), but the former has a lower standard deviation. This fact indicates that the stronger deuterium bonds are stabilizing the active-site solvent cluster to an appreciable extent. However, the degree of stabilization is not enough to alter the cluster distribution in this particular system. Therefore, it is concluded that the deuterium and protium systems involve similarly sized clusters in the rate-limiting PT event. Given this information and our recent PMF for the PT in the WT enzyme,[6] an atomistic description of the KIE is possible. Recent MS-EVB simulations of the WT HCA II including His64 in both the inward and outward orientations have found that the barrier for the PMF describing the PT event was best characterized by an Eigen cation ($H_9O_4^+$),[6] consistent with WT HCA II KIE experiments that indicate changes in bonding to many hydrogen atoms.[15] Due to the presence of an Eigen complex at the transition state in the WT PMF's for both the inward and outward orientations, similar KIE values would be predicted for both WT systems. Indeed, if the WT PMF for His64 in the outward orientation is used to describe the PT event in the N67L mutant, similar KIE values would be predicted for both the WT and N67L HCA II, as is found experimentally (see Supplemental Information for a more detailed description of this analysis).

Hydration pathway (ZnH_2O^{2+}-His)

While our experimental data have focused on the dehydration pathway of the N67L mutant, its hydration pathway is also important in understanding the full effect of the mutation on the inward/outward orientation of His64, water cluster characteristics, and the observed rate. Simulation results from the χ1 dihedral PMF (Figure 3A) indicate that for the hydration reaction, His64 is equally likely to be in either orientation. To study the role of His64 orientation during the rate-limiting PT event, we analyzed the water cluster size, distribution water cluster lifetimes, and the correlations between various types of water clusters and amino acids. Water cluster size distributions and probabilities are comparable for the N67L mutant and WT enzyme, for both inward and outward orientations of His64,[13] although the N67L mutant clusters have significantly greater variance. The lifetimes of the water clusters for the hydration system indicate that the mutation at position 67 has significantly altered the ability of the enzyme to stabilize water clusters for an appreciable amount of time when His64 is in the inward orientation (≤ 0.8 ps). The corresponding water cluster lifetimes for the WT enzyme are between 1 and 6 ps.[13] It is of note that when His64 is in the outward orientation, the water

cluster sizes and lifetimes for WT and N67L are similar, further indicating no significant change between WT and N67L when His64 adopts the outward orientation.

From the correlation analysis, it seems clear that the degree of correlation between the water clusters and the surrounding amino acids for the inward orientation of N67L is reduced compared to correlations observed in the WT system.[13] The lack of correlation results in an enzyme with a reduced ability to stabilize any active-site water clusters. This idea is in line with our earlier data showing that the N67L mutant forms water clusters that are unstable and short-lived compared to the WT system, despite having about the same size distribution. For the hydration pathway with His64 in the outward orientation, little correlation between the water cluster and the surrounding amino acids is present. This absence of stabilizing hydrogen bonding is similar to that seen in the corresponding WT system, and is also reflected in the occupancy plots which indicate disorder in the active site. Even though disorder occurs, PT is possible as seen in the WT, but with a reduced overall rate.

These results indicate that when His64 is in the inward orientation for the N67L mutant, the instability and short lifetime of the water clusters connecting proton donor and acceptor preclude a significant contribution of the inward orientation of His64 to the overall rate of PT, thereby favoring PT through systems with His64 in the outward orientation. It is this preference for the outward orientation which is reasoned to cause the somewhat elevated barrier to PT. Although the degree of preference is difficult to quantify, our observations are in agreement with the experimental observation that the PT rate constant is four times less in N67L than in WT. These results stress the importance of evaluating not only the orientation of His64 but also the active-site water cluster characteristics. A simple prediction that the orientation of His64 should be around 50/50 is not enough to dictate the use of a specific or exclusive orientation in this particular system. Evaluation of the active-site water cluster characteristics is valuable to help determine if a particular orientation of His64 is viable for PT.

Conclusions

This work has increased our knowledge of the driving forces behind the HCA II PT mechanism and its rate in the N67L mutant. Furthermore, it has shown that to fully understand the impact of specific mutations on an observed rate, the orientational stability of His64 and the active-site water cluster characteristics are important to taken into account. In the dehydration system of the N67L mutant the His64 side chain is predominantly in the outward orientation, but this does not drastically alter the observed rate, causing only a four-fold reduction. Analysis of the active-site water cluster has shown significant similarities between the WT and N67L HCA II, indicating that the mutation has not inhibited the enzyme's ability to create a favorable environment for PT. Indeed, the reduction in the rate can likely be attributed to the PT event proceeding through a water cluster connecting the donor and acceptor when His64 is in the outward orientation, as seen supported by recent simulations.[6] Further analysis has revealed that for the hydration reaction, the mutation has significantly disrupted the water cluster when His64 is in the inward orientation, thereby causing the enzyme to utilize His64 in the outward orientation for PT. The use of the outward orientation for the hydration reaction as well as for the dehydration reaction is in agreement with experiment, which indicates a reduced rate of dehydration in the N67L mutant relative to the WT. While the observed rate is affected by the N67L mutant as compared to WT, the mechanism of PT is unchanged. Kinetic and simulation data further indicate that the transition states for both the WT and the N67L mutant are occupied by an Eigen cation. The notion of an Eigen cation at the transition state is in line with the observed KIE results for both the WT and N67L mutant.

Supplementary Material

Refer to Web version on PubMed Central for supplementary material.

Acknowledgments

This work was supported by a grant from the NIH GM25154 and research funds from the University of Florida for DNS and RM. The computational research was supported by the NIH (GM53148) for GAV. The computational resources have been provided in part by the National Institute of Health (Grant # NCRR 1 S10 RR17214-01) on the Arches Metacluster administered by the University of Utah Center for High Performance Computing.

Abbreviations

PT
proton transfer

HCA II
human carbonic anhydrase II

MD
molecular dynamics

WT
wild-type

KIE
kinetic isotope effect

PIMD
path integral molecular dynamics

CA
carbonic anhydrase

PDB
protein data bank

NMPIMD
normal mode path integral molecular dynamics

PMF
potential of mean force

WHAM
weighted histogram analysis method

MS-EVB
multi-state empirical valence bond

References

1. Silverman DN, Lindskog S. The Catalytic Mechanism of Carbonic Anhydrase: Implications of a Rate-Limiting Protolysis of Water. Acc Chem Res 1988;21(1):30–36.
2. Christianson DW, Fierke CA. Carbonic Anhydrase: Evolution of the Zinc Binding Site by Nature and by Design. Acc Chem Res 1996;29(7):331–339.
3. Lindskog S. Structure and Mechanism of Carbonic Anhydrase. Pharmacol Ther 1997;74(1):1–20. [PubMed: 9336012]

4. Tu C, Silverman DN, Forsman C, Jonsson BH, Lindskog S. Role of histidine 64 in the catalytic mechanism of human carbonic anhydrase II studied with site-specific mutant. Biochemistry 1989;28 (19):7913–7918. [PubMed: 2514797]
5. Steiner H, Jonsson BH, Lindskog SJ. The Catalytic Mechanism of Carbonic Anhydrase. Hydrogen Isotope Effects on the Kinetic Parameters of the Human C Isoenzyme. Eur J Biochem 1975;59(1): 253–259. [PubMed: 1249]
6. Maupin CM, McKenna R, Silverman DN, Voth GA. Elucidation of the Proton Transport Mechanism in Human Carbonic Anhydrase II. J Am Chem Soc 2008;131(22):7598–7608. [PubMed: 19438233]
7. Liljas A, Kannan KK, Bergsten PC, Waara I. Crystal structure of human carbonic anhydrase C. Nature 1972;235:131–137.
8. Nair SK, Christianson DW. Unexpected pH-dependent conformation of His-64, the proton shuttle of carbonic anhydrase II. J Am Chem Soc 1991;113:9455–9458.
9. Silverman DN, McKenna R. Solvent-Mediated Proton Transfer in Catalysis by Carbonic Anhydrase. Acc Chem Res 2007;40:669–675. [PubMed: 17550224]
10. Kresge AJ, Silverman DN. Application of Marcus rate theory to proton transfer in enzyme-catalyzed reactions. Enzyme Kinetics and Mechanism, Pt E 1999;308:276.
11. Fisher Z, Hernandez Prada JA, Tu C, Duda D, Yoshioka C, An H, Govindasamy L, Silverman DN, McKenna R. Structural and Kinetic Characterization of Active-Site Histidine as a Proton Shuttle in Catalysis by Human Carbonic Anhydrase II. Biochemistry 2005;44(4):1097–1105. [PubMed: 15667203]
12. Fisher SZ, Tu C, Bhatt D, Govindasamy L, Agbandje-McKenna M, McKenna R, Silverman DN. Speeding Up Proton Transfer in a Fast Enzyme: Kinetic and Crystallographic Studies on the Effect of Hydrophobic Amino Acid Substitutions in the Active Site of Human Carbonic Anhydrase II. Biochemistry 2007;46:3803–3813. [PubMed: 17330962]
13. Maupin CM, Saunders MG, Thorpe IF, McKenna R, Silverman DN, Voth GA. Origins of Enhanced Proton Transport in the Y7F Mutant of Human Carbonic Anhydrase II. J Am Chem Soc 2008;130 (34):11399–11408. [PubMed: 18671353]
14. Schowen KS, Schowen RL. Solvent Isotope Effects on Enzymes-Systems. Methods in Enzymology 1982;87:551–606. [PubMed: 6294457]
15. Venkatasubban KS, Silverman DN. Chemical rescue in catalysis by human carbonic anhydrase II and III. Biochemistry 1980;41(9):3235–3242.
16. An H, Tu C, Duda D, Montanez-Clemente I, Math K, Laipis PJ, McKenna R, Silverman DN. Chemical Rescue in Catalysis by Human Carbonic Anhydrase II and III. Biochemistry 2002;41(9):3235–3242. [PubMed: 11863462]
17. Khalifah RG. Histidine-200 Alters Inhibitor Binding in Human Carbonic Anhydrase B - C-13 Nuclear Magnetic Resonance Identification. Biochemistry 1977;16:2236–2240. [PubMed: 405036]
18. Segel, IH. Enzyme Kinetics. Wiley-Interscience; New York: 1975.
19. Silverman DN. Carbonic Anhydrase: Oxygen-18 Exchange Catalyzed by an Enzyme with Rate-Contributing Proton-Transfer Steps. Methods Enzymol 1982;87:732–752. [PubMed: 6294458]
20. Silverman DN, Tu C, Chen X, Tanhauser SM, Kresge AJ, Laipis PJ. Rate-Equilibria Relationships in Intramolecular Proton Transfer in Human Carbonic Anhydrase III. Biochemistry 1993;32:10757–10762. [PubMed: 8399223]
21. Simonsson I, Jonsson BH, Lindskog S. C-13 NMR Study of Carbon Dioxide-Bicarbonate Exchange Catalyzed by Human Carbonic Anhydrase-C at Chemical Equilibrium. European Journal of Biochemistry 1979;93:409–417. [PubMed: 34514]
22. Håkansson K, Carlsson M, Svensson LA, Liljas A. Structure of Native and Apo Carbonic Anhydrase II and Structure of Some of its Anion-Ligand Complexes. J Mol Biol 1992;227(4):1192–1204. [PubMed: 1433293]
23. Guex N, Peitsch MC. SWISS-MODEL and the Swill-Pdb Viewer: An environment for comparative protein modeling. Electrophoresis 1997;18:2714–2723. [PubMed: 9504803]
24. Day TJ, Soudackov AV, Cuma M, Schmitt UW, Voth GA. A Second Generation Multistate Empirical Valence Bond Model for Proton Transport in Aqueous Systems. J Chem Phys 2002;117(12):5839–5849.

25. Wang J, Cieplak P, Kollman PA. How well does a restrained electrostatic potential (RESP) model perform in calculating conformational energies of organic and biological molecules? J Comput Chem 2000;21(12):1049–1074.
26. Maupin CM, Voth GA. Preferred Orientations of His64 in Human Carbonic Anhydrase II. Biochemistry 2007;46(11):2938–2947. [PubMed: 17319695]
27. Kast SM, Nicklas K, Bär HJ, Brickmann J. Constant Temperature Molecular Dynamics Simulations by Means of a Stochastic Collision Model. I. Noninteracting Particles. J Chem Phys 1994;100(1): 566–576.
28. Hummer G, Pratt LR, Garcia AE. Free Energy of Ionic Hydration. J Phys Chem 1996;100(4):1206–1215.
29. Major DT, Garcia-Viloca M, Gao J. Path Integral Simulations of Proton Transfer Reactions in Aqueous Solution Using Combined QM/MM Potentials. J Chem Theory Comput 2006;2:236–245.
30. Feierberg I, Luzhkov V, Aqvist J. Computer Simulation of Primary Kinetic Isotope Effects in the Proposed Rate-limiting Step of the Glyoxalase I Catalyzed Reaction. J Biol Chem 2000;275:22657–22662. [PubMed: 10801792]
31. Liu H, Warshel A. Origin of the Temperature Dependence of Isotope Effects in Enzymatic Reactions: The Case of Dihydrofolate Reductase. J Phys Chem B 2007;111:7852–7861. [PubMed: 17571875]
32. Hwang JK, Warshel A. How important are quantum mechanical nuclear motions in enzyme catalysis? J Am Chem Soc 1996;118:11745–11751.
33. Case, DA.; D, TA.; Cheatham, TE., III; Simmerling, CL.; Wang, J.; Duke, RR.; Luo, R.; Crowley, M.; Walker, RC.; Zhang, W.; Merz, KM.; Wang, B.; Hayik, S.; Roitberg, A.; Seabra, G.; Kolossvαry, I.; Wong, KF.; Paesani, F.; Vanicek, J.; Wu, X.; Brozell, SR.; Steinbrecher, T.; Gohlke, H.; Yang, L.; Tan, C.; Mongan, J.; Horn, V.; Cui, G.; Mathews, DH.; Seetin, MG.; Sagui, C.; Babin, V.; Kollman, PA. AMBER. Vol. 10. University of California; San Francisco: 2008.
34. Tuckerman, ME. Path Integration via Molecular Dynamics. In: Grotendorst, J.; Marx, D.; Muramatsu, A., editors. Quantum Simulations of Complex Many-Body Systems: From Theory to Algorithms. Vol. 10. John von Neumann Institute for Computing; Jülich, Germany: 2002. p. 269
35. Berne BJ, Thirumalai D. On the simulation of quantum systems: path integral methods. Annu Rev Phys Chem 1986;37:401–424.
36. Martyna G, Klein M, Tuckerman M. Nosé-Hoover chains: The canonical ensemble via continuous dynamics. J Chem Phys 1992;97
37. Paesani F, Zhang W, Case DA, Cheatham TE, Voth GA. An accurate and simple quantum model for liquid water. J Chem Phys 2006;125:184507–184511. [PubMed: 17115765]
38. Humphrey W, Dalke A, Schulten K. VMD - Visual Molecular Dynamics. J Molec Graphics 1996;14:33–38.
39. Kumar S, Bouzida D, Swendsen RH, Kollman PA, Rosenberg JM. The Weighted Histogram Analysis Method for Free-Energy Calculations on Biomolecules. I. The Method. J Comput Chem 1992;13(8): 1011–1021.
40. Roux B. The Calculation of the Potential of Mean Force using Computer Simulations. Comput Phys Commun 1995;91:275–282.
41. Duda D, Tu C, Qian M, Laipis P, Agvandje-McKenna A, Silverman DN, McKenna R. Structural and Kinetic Analysis of the Chemical Rescue of the Proton Transfer Function of Carbonic Anhydrase II. Biochemistry 2001;40(6):1741–1748. [PubMed: 11327835]
42. Scheiner S, Cuma M. Relative Stability of Hydrogen and Deuterium Bonds. J Am Chem Soc 1996;118:1511–1521.
43. Cuma M, Scheiner S. Influence of isotopic substitution on strength of hydrogen bonds of common organic groups. Journal of Physical Organic Chemistry 1997;10:383–395.
44. Toba S, Colombo G, Merz KM Jr. Solvent Dynamics and Mechanism of Proton Transfer in Human Carbonic Anhydrase II. J Am Chem Soc 1999;121(10):2290–2302.
45. Zheng J, Avvaru BS, Tu C, McKenna R, Silverman DN. Role of Hydrophobic Residues in Proton Transfer During Catalysis by Human Carbonic Anhydrase II. Biochemistry 2008;47(46):12028–12036. [PubMed: 18942852]

46. Krebs JF, Fierke CA, Alexander RS, Christianson DW. Conformational Mobility of His64 in the Thr200Ser Mutant of Human Carbonic Anhydrase II. Biochemistry 1991;30(38):9153–9160. [PubMed: 1909891]

47. Riccardi D, Konig P, Guo H, Cui Q. Proton Transfer in Carbonic Anhydrase Is Controlled by Electrostatics Rather than the Orientation of the Acceptor. Biochemistry 2008;47:2369–2378. [PubMed: 18247480]

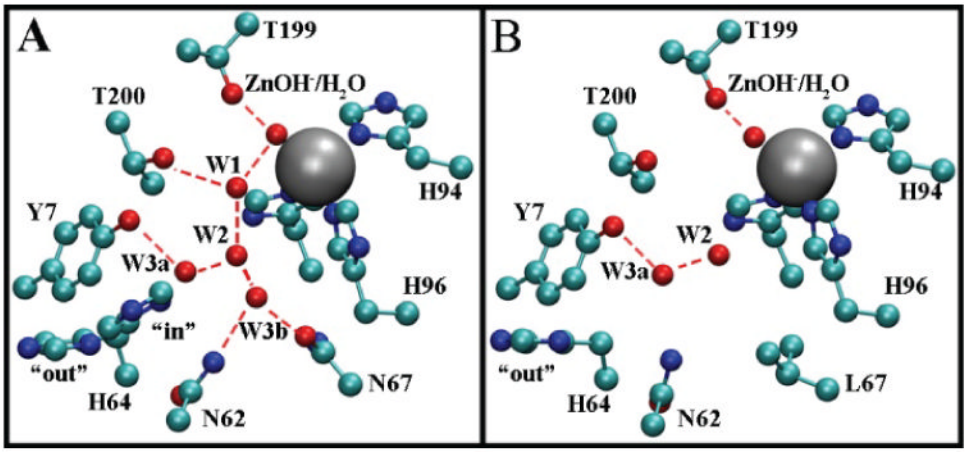

Figure 1.

The active site of (A) WT and (B) N67L HCA II taken from the crystal structures of Fisher *et al*.[12] Red spheres represent ordered water molecules and are numbered (W1, W2, W3a, W3b), and red dashed lines indicate distances consistent with hydrogen bonds (2.6 – 3.2 Å). The side chain of His64 is shown in both the inward and outward conformation in the WT (A), but exists only in the outward conformation in N67L(B).

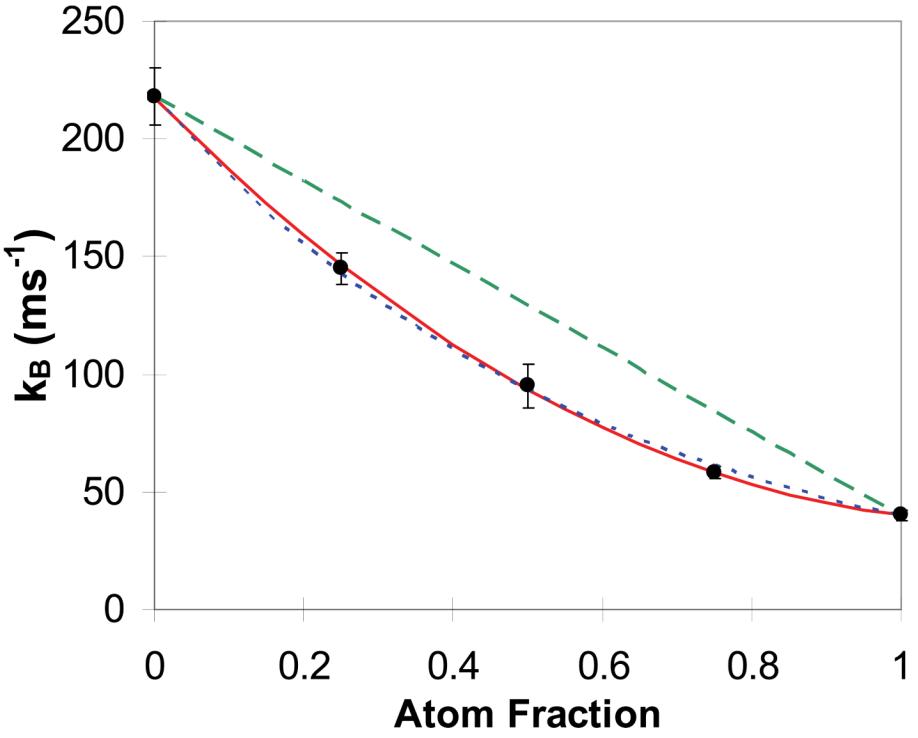

Figure 2.

The rate constants for proton transfer k_B as a function of atom fraction of deuterium in solvent for catalysis by N67L HCA II. The lines represent (*green*) a linear dependence; and (*blue*) a logarithmic dependence on the atom fraction of deuterium in solvent. The red line and black circles represents the experimental data. Solutions contained 25 mM of all species of CO_2 at 10 °C, sufficient Na_2SO_4 to maintain 0.2 M ionic strength, and no added buffers.

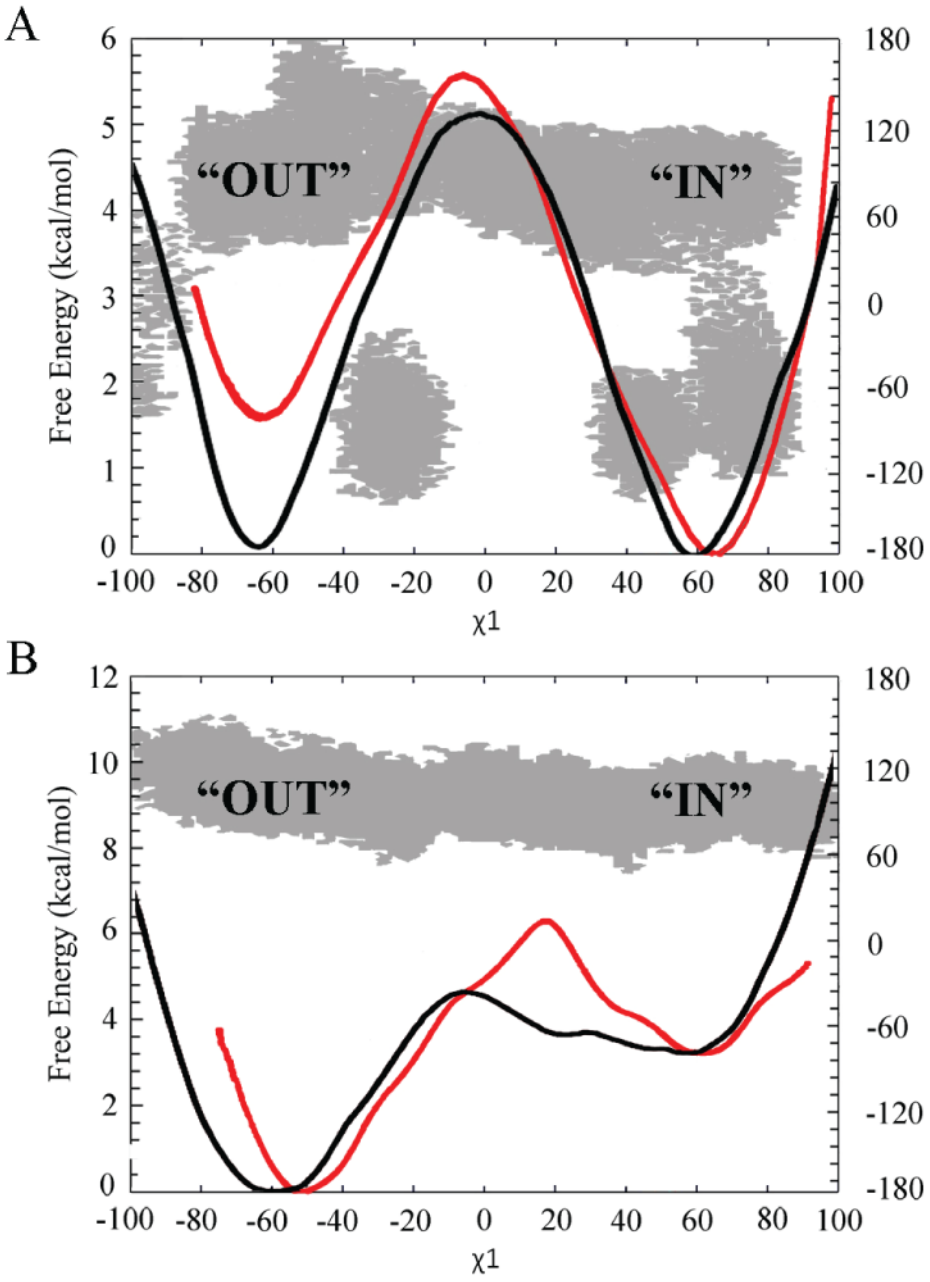

Figure 3.

Free energy profile (PMF) for the rotation of His64 about the χ1 dihedral angle in N67L (*black*) and WT (*red*) HCA II[26]: (A) for the hydration (ZnH_2O^{2+}-His) system; and (B) for the dehydration ($ZnOH^{+}$-$HisH^{+}$) system. The sampled distribution of the His64 about the χ2 dihedral angle is represented by the grey area. The error of the curves estimated by bootstrap error analysis and box car averaging is ≤ 0.2 kcal/mole.

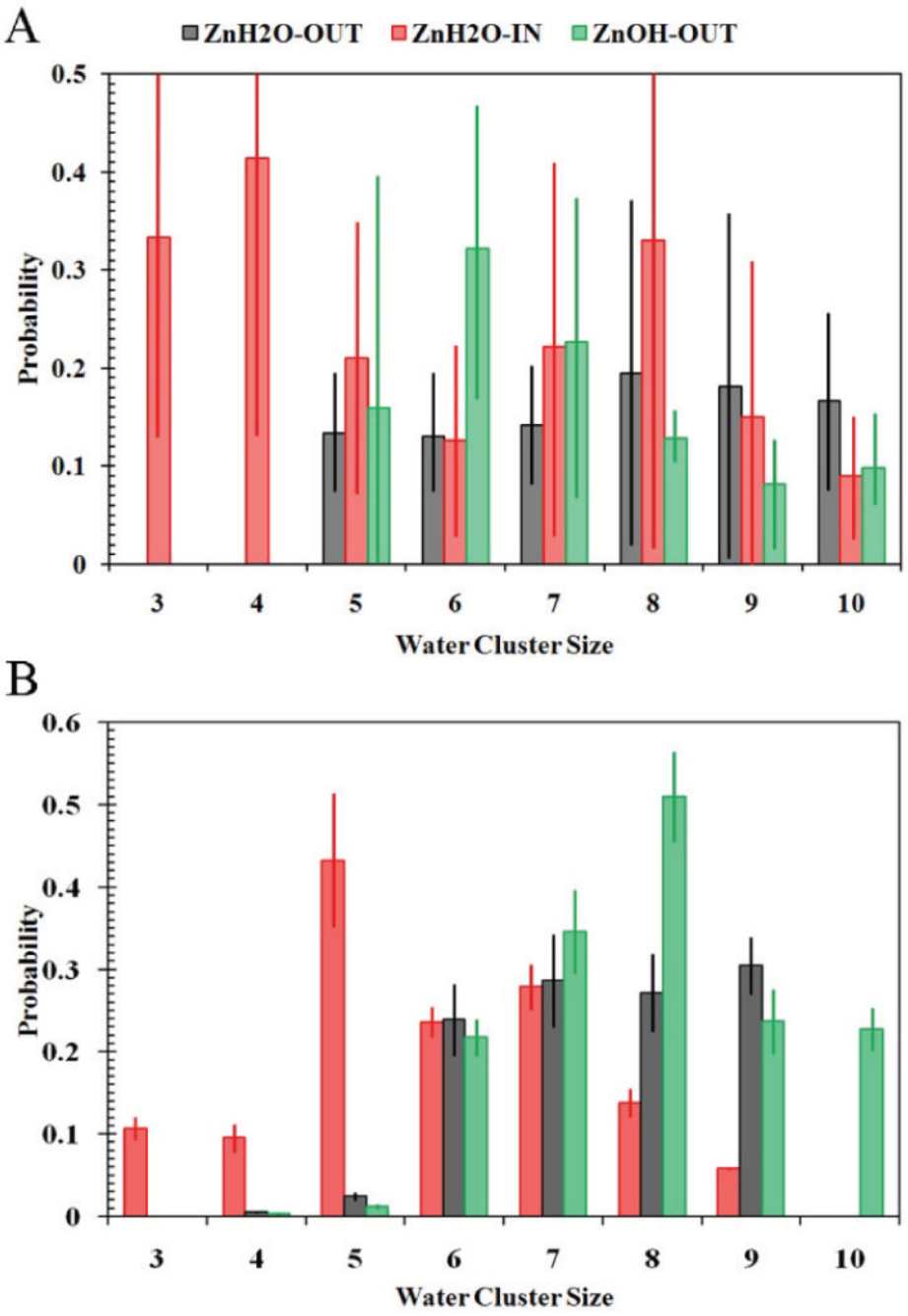

Figure 4.

Histogram for size of water clusters in the active-site cavity of N67L HCA II. (*red*) Hydration (ZnH_2O^{2+}-His) system with His64 in the inward orientation; (*black*) hydration system with His64 in the outward orientation; and (*green*) dehydration ($ZnOH^+$-$HisH^+$) system with His64 in the outward orientation: for the H_2O system (A); and the D_2O system (B).

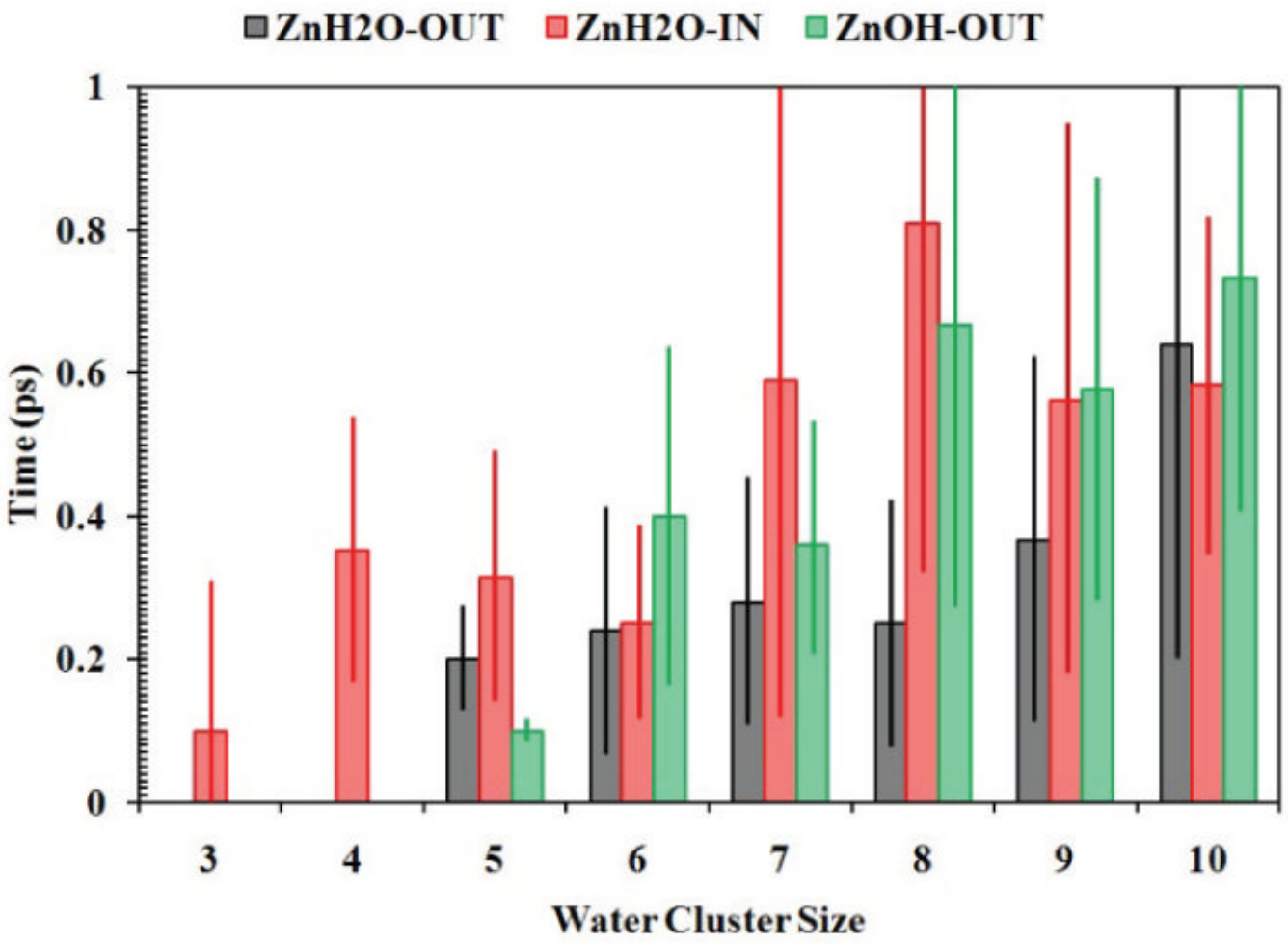

Figure 5.

Histogram for lifetime of water clusters in the active-site cavity of N67L HCA II. (*red*) Hydration (ZnH_2O^{2+}-His) system with His64 in the inward orientation; (*black*) hydration system with His64 in the outward orientation; and (*green*) dehydration ($ZnOH^{+}$-$HisH^{+}$) with His64 in the outward orientation.

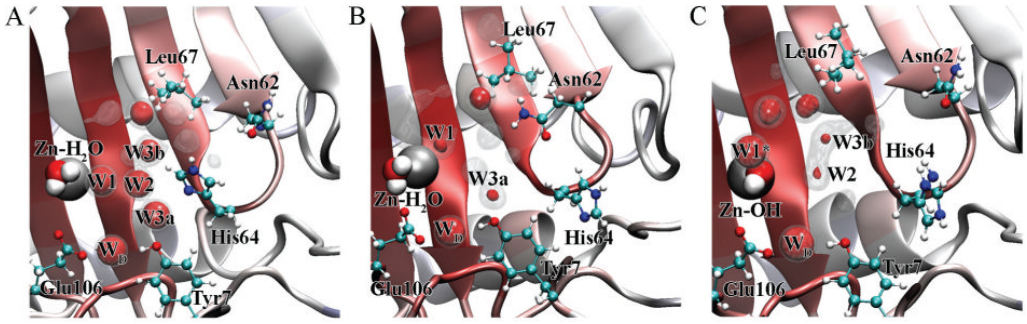

Figure 6.

Occupancy of water clusters in the active-site cavity of N67L HCA II. The red surfaces correspond to the 75% isosurface, while the transparent surface corresponds to the 50% isosurface. (A and B) hydration (ZnH_2O^{2+}-His) systems with His64 in the inward and outward orientations, respectively; and (C) the dehydration ($ZnOH^{+}$-$HisH^{+}$) system with His64 in the outward orientation for the classical MD simulation. Due to the absence of a stabilized water in the typical W1 position, W1* was selected as the most stable water hydrogen-bonded to the zinc-hydroxide.

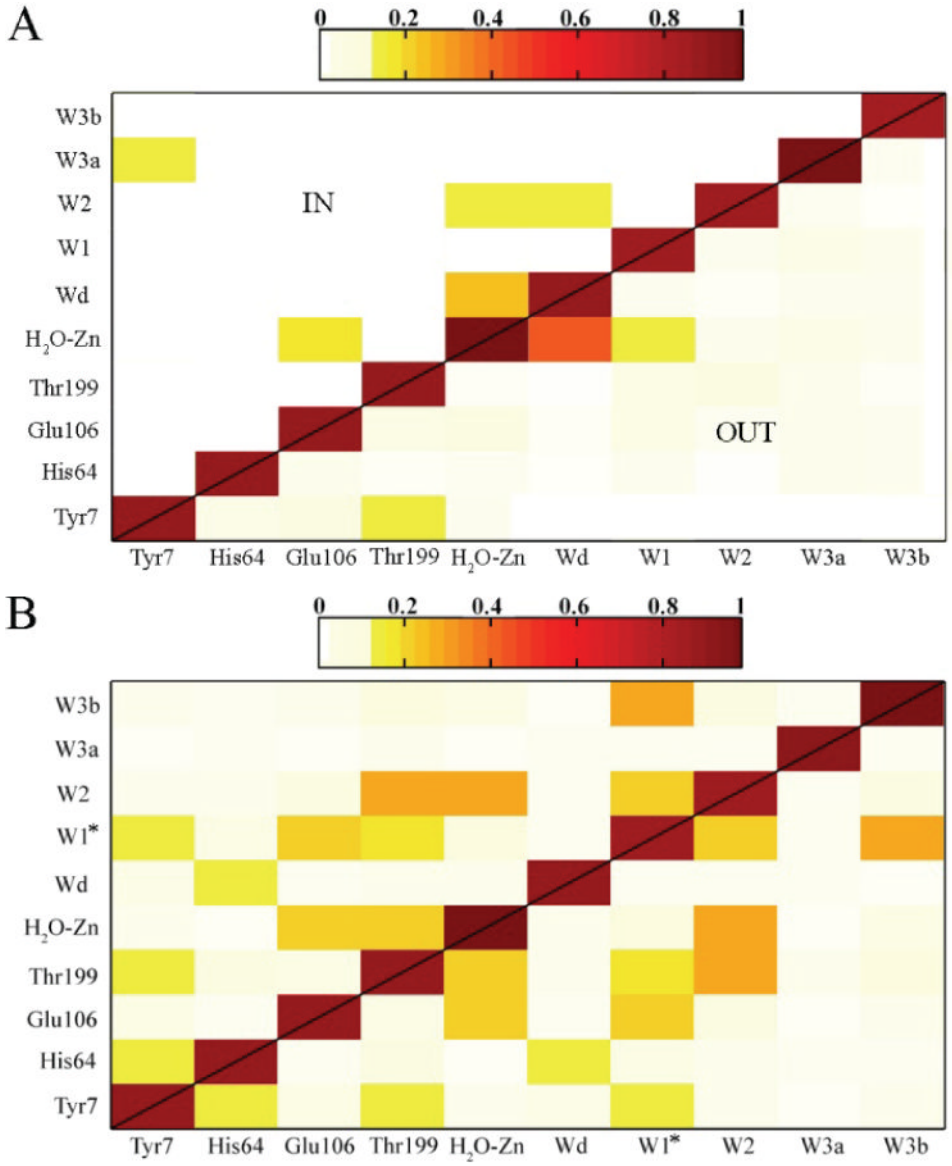

Figure 7.

Correlation analysis for the active-site water cluster and stabilizing amino acids in N67L. Hydration (ZnH_2O^{2+}-His) system with His64 in the inward orientation (A top left), hydration system with His64 in the outward orientation (A bottom right), and dehydration ($ZnOH^+$-$HisH^+$) system with His64 in the outward orientation (B). Due to the absence of a stabilized water in the typical W1 position, W1* was selected as the most stable water hydrogen-bonded to the zinc-hydroxide.